The Astrophysical Journal, 655:1142–1156, 2007 February 1

IN/OUT PAIRS AND THE DETACHMENT OF CORONAL STREAMERS

N. R. Sheeley, Jr. and Y.-M. Wang
E. O. Hulburt Center for Space Research, Naval Research Laboratory, Washington DC;
sheeley@spruce.nrl.navy.mil, ywang@yucca.nrl.navy.mil
Received 2006 June 27; accepted 2006 October 19

ABSTRACT

We previously described coronal events that originate in the 2–6 $R_\odot$ field of view of the LASCO white-light coronagraph and involve the simultaneous ejection of material inward toward the Sun and outward away from it. Now, in a study of more than 160 in/out pairs, we have found that these features are density enhancements at the leading and trailing edges of depletions that occur when slowly rising coronal structures separate from the Sun. The outward component is shaped like a large arch with both ends attached to the Sun, and the inward component is often resolved into loops. We also found about 60 additional events in which the outward components began near the edge of the occulting disk and inward components were not visible, as if these events were in/out pairs that originated below the 2 $R_\odot$ radius of the occulting disk. We conclude that in/out pairs belong to a broad class of streamer detachments, which include "streamer blowout" coronal mass ejections, and we suppose that all of these events occur when rising magnetic loops reconnect to produce an outgoing helical flux rope and an ingoing arcade of collapsing loops.

Subject headings: Sun: corona — Sun: coronal mass ejections (CMEs) — Sun: magnetic fields

1. INTRODUCTION

This paper describes observations obtained with the Large Angle Spectrometric Coronagraph (LASCO) on the *Solar and Heliospheric Observatory* (*SOHO*). LASCO includes two white-light coronagraphs (C2 and C3) with separate fields of view spanning the ranges 2–6 and 4–30 $R_\odot$, respectively, and has observed a variety of coronal structures and transients since operations began in early 1996. In addition to coronal mass ejections (CMEs) and outward moving streamer "blobs," we have observed more than 10,000 small and usually faint features moving toward the Sun. About 98% of these coronal inflows occur in long-lived streams at north-south excursions of the streamer belt. These raining inflows seem to indicate the ongoing magnetic field line reconnection that occurs as differential rotation shears the photospheric neutral line, weakens the equatorial component of the Sun's dipole field, and gradually flattens the streamer belt (Sheeley et al. 2001; Sheeley & Wang 2001). Like the inflows above postflare loops (McKenzie & Hudson 1999; McKenzie 2000; Gallagher et al. 2002; Innes et al. 2003a, 2003b; Asai et al. 2004; Sheeley et al. 2004), these raining inflows do not have visible outward components, perhaps because they are faint and headed upward into regions of even lower density.

About 2% of the LASCO inflows (~160) are accompanied by outward components (Wang et al. 1999; Sheeley & Wang 2002; Simnett 2004). Unlike the raining inflows, which become less dense than their surroundings as they move inward, the separating components of in/out pairs are density enhancements. In addition, their outward components have characteristic arch-shaped signatures. In a recent paper of this series (Wang & Sheeley 2006, hereafter Paper I), we described observations and simulations that suggest that the outward component has the helical structure of a magnetic flux rope.

A puzzling aspect of the in/out pairs has been their origin. Unlike raining inflows, which were visible whenever a north-south segment of the streamer belt rotated past the east or west limb, the in/out pairs occurred sporadically with no apparent relation to magnetic structures or the occurrence of CMEs. Some in/out pairs seemed to be triggered by shock waves from major CMEs, but many of them did not. Now, in a study of 162 in/out pairs, we have found that at least 80% are preceded by a 1–2 day interval of gradual coronal expansion, which ends with the onset of the pair. (The remaining 20% are distributed evenly between indeterminate cases and cases for which the pair lies in the wake of a sequence of CMEs.) In the next section of this paper, we describe this new discovery and show additional events that may be in/out pairs that originate below the occulting disk, where the inward components are not visible. In the final section, we summarize these observations and interpret them in terms of a rising arcade of loops that reconnect to form an outgoing helical flux rope and an ingoing system of collapsing loops.

2. OBSERVATIONS

2.1. *In/Out Pairs and Streamer Disconnection Events*

Figure 1 shows eight sets of C2 and C3 images of in/out pairs observed during the years 2000–2005, arranged in decreasing order of their apparent size. Each frame contains a running difference image, obtained by subtracting the previous image on that day from the current image. Such difference images show subtle proper motions without the distracting effects of stationary background features. In the first few C2 frames, the in/out pairs appear as oppositely directed arches resembling the jaws of an open mouth. The C3 images show the outward components a few hours later as large arches whose legs extend back toward the Sun. As we have discussed previously, the inward and outward components move at speeds of about 100 and 300 km s^{-1}, respectively, relative to the center of the Sun, and therefore separate from each other at relative speeds of about 400 km s^{-1} (Sheeley & Wang 2002). In these running difference images, the inward and outward components have the leading-white/trailing-black signatures of density enhancements, rather than the leading-black/trailing-white signatures of the dark loops and trailing "tadpole-like" features that accompany raining inflows.

As we look through the sequence of C2 images in Figure 1, we see a change in the apparent size of the jaw-like separations, as if we were obtaining a more oblique view of these events. Eventually, the pairs are so narrow that they resemble the streamer

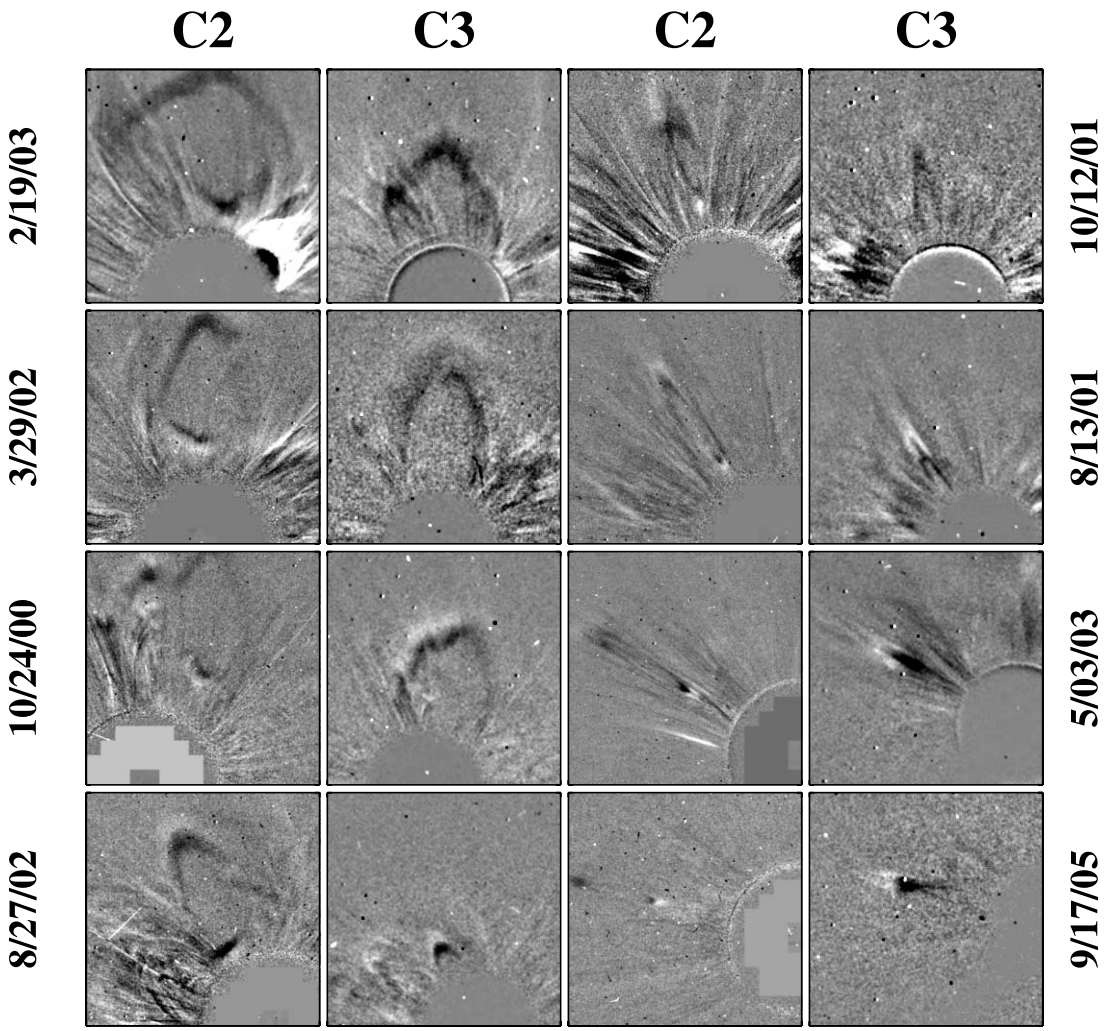

FIG. 1.—Running difference images, showing a selection of eight in/out pairs in the C2 field of view (cropped to 6 $R_\odot$ on a side) and the outward components of these pairs a few hours later in the C3 field (cropped to 15 $R_\odot$ on a side). These events are arranged in decreasing order of their angular spans to show the apparent trend from face-on to edge-on views.

disconnection events we observed during the rising phase of the sunspot cycle (Wang et al. 1999). As we show next, other properties of in/out pairs are also consistent with this idea that they are face-on views of streamer disconnection events.

2.2. *Spontaneous In/Out Pairs*

Figure 2 refers to an in/out pair on 2005 October 12. In the left column, the running difference images show the formation and initial separation of the inward and outward components as they move through the southwest quadrant of the C2 field of view (6 $R_\odot$ on each side). As usual, each component has the leading-white/trailing-black signature of a density enhancement. The middle column contains images obtained by subtracting a monthly minimum intensity from each pixel. By subtracting the monthly minimum intensity, we reduce the quasi-stationary contributions of scattered light from circumsolar dust and from the LASCO optical train, as we did with the running difference images, but without removing the contributions of coronal streamers.

These "minimum subtracted" images show a dark depletion between the ingoing and outgoing components of the pair. Because the depletion expands rapidly, its edges overtake and compress material that lies ahead, causing the density enhancements that give rise to the leading-white/trailing-black signatures in running difference images. While the inward component has a spiny shape similar to that of a postflare loop system, the outgoing component has a corrugated, cusplike shape, consistent with the helical topology of a flux rope, as described in Paper I. In the right column, similar minimum-subtracted images show the depletion as it continues outward through the C3 field of view (cropped to 15 $R_\odot$ on each side). Clearly, this in/out pair left the corona less dense than it was before.

Figure 3 shows height/time maps, obtained by observing the evolution of the in/out pair through a radial slit and then placing the resulting strips in chronological order. This procedure has been described previously by Sheeley et al. (1999). In general, we chose a slit width of 17 pixels, but for one particularly complicated event (2004 January 20, shown in Figs. 6–9), we increased the width to 25 pixels to capture the details of the motion. Running difference images were used in the top panel, which tracks spatial fluctuations of coronal intensity as they move through the field of view. A 36 hr interval of gradual acceleration from an initial speed $\sim$20 km s^{-1} ends with the sudden formation of the in/out pair. The tracks of the inward and outward components appear as a trailing boundary of the flow field, which does not extend beyond them. The slope of the upward boundary is approximately 360 km s^{-1}.

The bottom panel of Figure 3 contains a height/time map, obtained using difference images relative to a fixed "base frame" near the start of the expansion, and indicates the accumulated

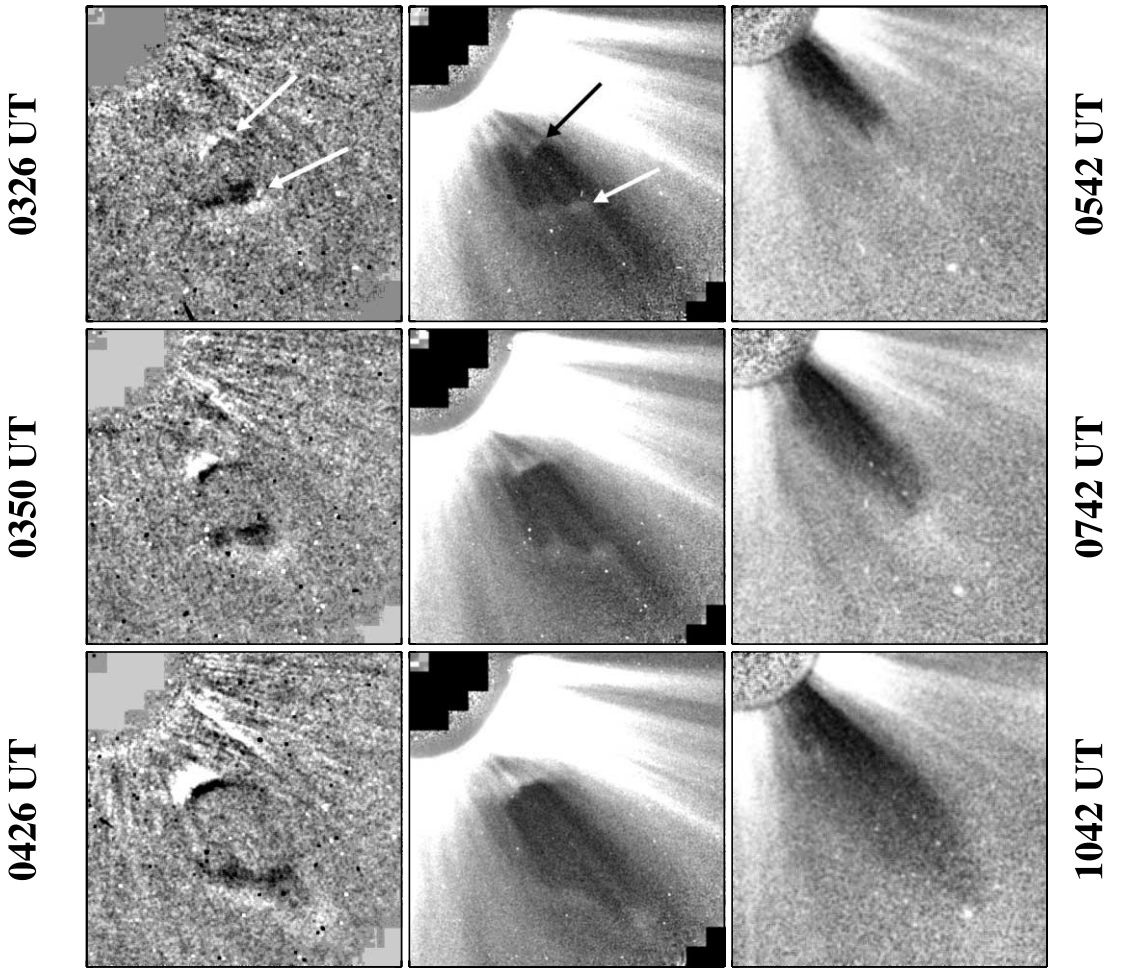

FIG. 2.—C2 running difference images (*left*) and the corresponding minimum-subtracted images (*center*) of an in/out pair in the southwest quadrant of the corona on 2005 October 12. These images show that the in/out pair consists of a pair of density enhancements separated by an expanding density depletion. C3 minimum-subtracted images (*right*) show the continued expansion of this depletion farther out in the corona. All of the C3 images in this paper have been cropped to 15 $R_\odot$ on a side

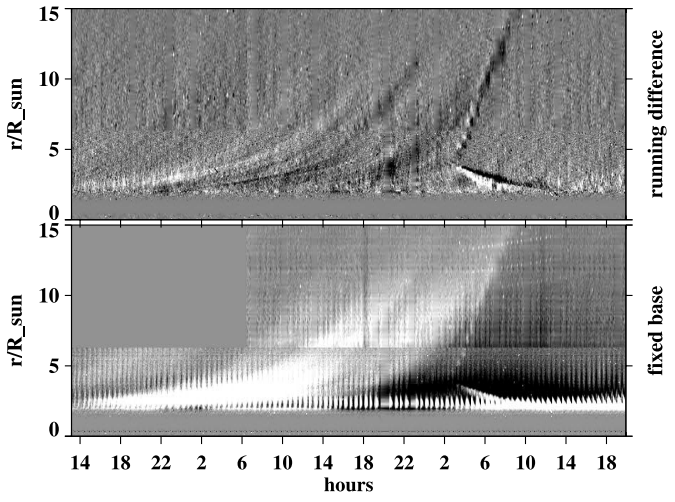

FIG. 3.—Height/time maps constructed from running difference images (*top*) and difference images relative to a fixed base near the start of the gradual expansion (*bottom*). The 36 hr interval (2005 October 10–12) of gradual expansion ends with the formation of the in/out pair. The position angle is 221°.

changes since that time. This map shows the slowly rising regions of coronal intensity, whose spatial fluctuations produced the tracks in the top panel. The pair leaves a darker corona in its wake.

Figures 4 and 5 refer to a very narrow in/out pair whose angular span was only 4°. This narrow 2005 September 17 pair is the last pair illustrated in Figure 1. In the C3 images of Figure 4 (*right*), the outward components resemble the "streamer blobs" that we studied during the rising phase of the sunspot cycle (Sheeley et al. 1997). Thus, it is natural to ask whether streamer blobs may be in/out pairs whose inward components are unobserved below the occulting disk. We think this is unlikely. Streamer blobs emerge from the tips of helmet streamers without leaving inward components behind. They also accelerate gradually and reach their terminal speeds of 300–400 km s^{-1} beyond 15 $R_\odot$ from Sun center. By comparison, the height/time maps in Figure 5 show that the outward component on September 17 started abruptly near 5 $R_\odot$ with a relatively high speed of 300 km s^{-1} and was accompanied by a prominent inward component. Presumably, these differences have a physical origin; the blobs are thought to be formed by reconnection between open and closed field lines (Wang et al. 1998), whereas the in/out pairs probably indicate reconnection between the closed loops of a rising arcade (Paper I).

In the top panel of Figure 5, the tracks of the gradual expansion are particularly well resolved and last for about 30 hr before the pair forms. In the upper branch, the tracks lose their identity

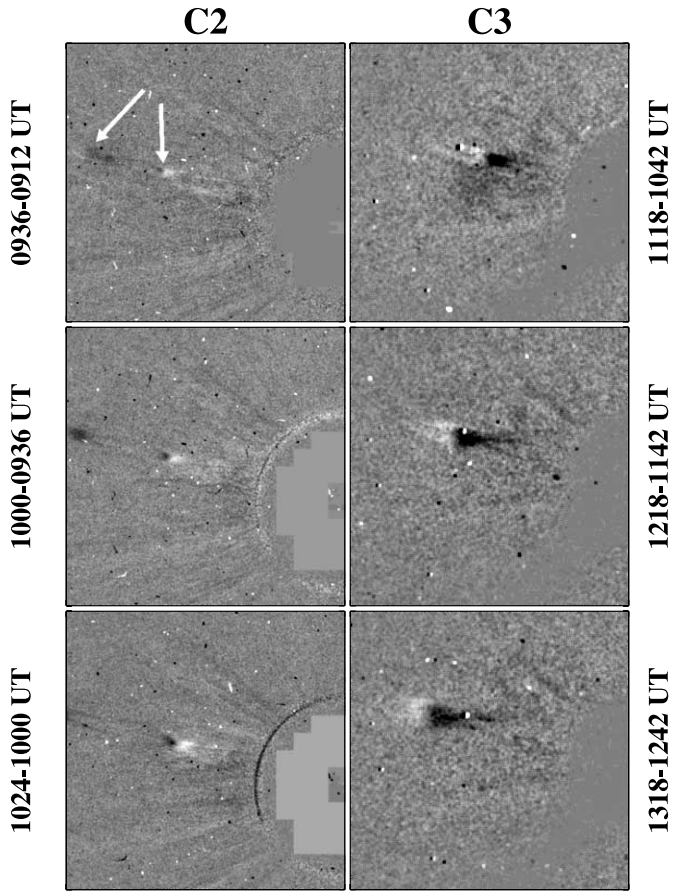

FIG. 4.—C2 (*left*) and C3 (*right*) running difference images of a very narrow in/out pair on 2005 September 17. The arrows indicate the inward and outward components near the start of the event at 09:36 UT.

when they encounter and merge with the steeper track of the outward component. In the lower branch, the tracks lose their identity when they encounter and merge with the track of the inward component. This behavior is unaffected by a CME whose short, steep track cuts across the pattern at 15:00 UT on September 16.

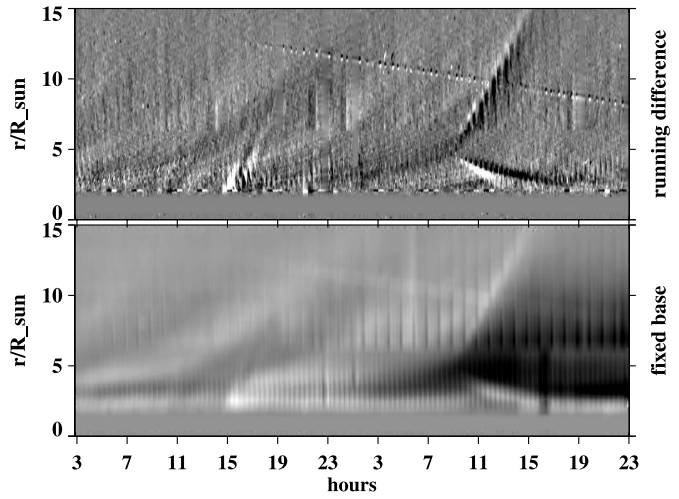

FIG. 5.—Height/time maps for the pair in Fig. 4, again showing that the pair marks the end of a long interval of coronal expansion. In particular, the individual tracks of the flow field continue both above and below the pair formation height until they reach the bounding tracks of the in/out pair. The fixed-base map has been smoothed to reduce periodic defects. The position angle is 75°.

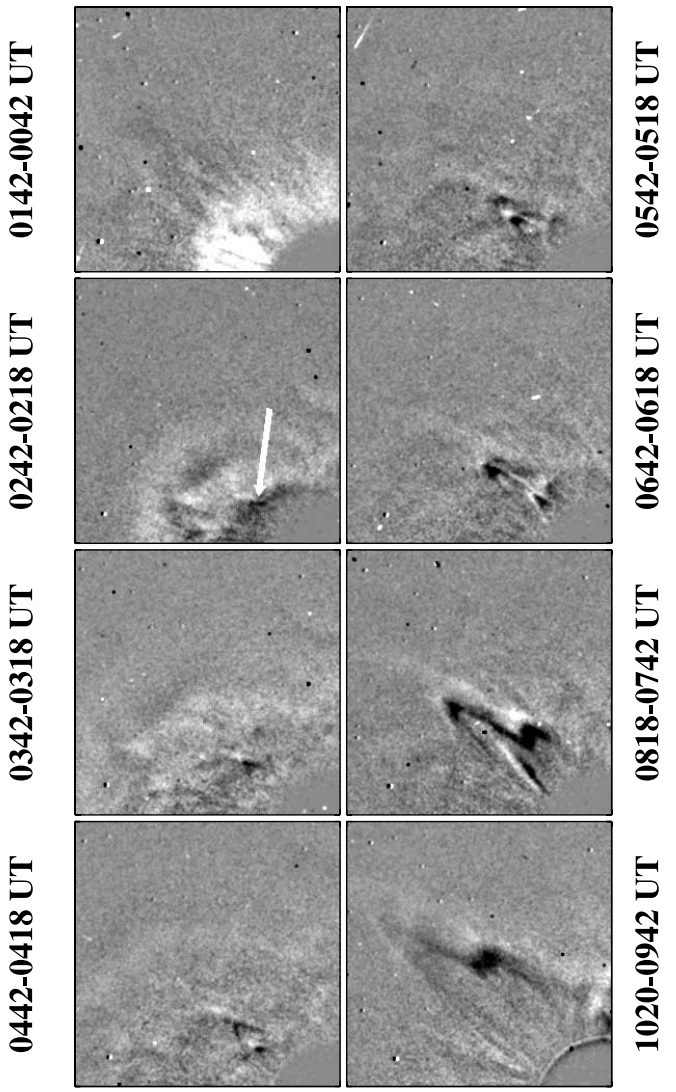

FIG. 6.—C3 running difference images of the northeast quadrant of the corona, showing the formation and merging of several "out components" in the wake of a halo CME on 2004 January 20. The arrow indicates the first of these arch-shaped features as it appears behind the disturbance from the CME.

In the bottom panel, the fixed-base height/time map shows the slowly rising intensity pattern, ending at the time of the pair. (We spatially smoothed this map to reduce periodic defects associated with the finite width of the stacked strips.)

2.3. *Pairs Triggered by CMEs*

The events we have just described occurred spontaneously without the perturbing effects of CMEs. However, sometimes the disturbance from a major CME will terminate streamer growth prematurely and trigger an in/out pair. From a subset of 60 well-observed in/out pairs, we found 30 events that seemed to be triggered by CMEs, 25 events that seemed to occur on their own, and five indeterminate events.

Next, we show an extreme case in which the disturbance from a halo CME on 2004 January 20 triggered a series of in/out pairs. Although the bulk of the ejected mass went into the southern hemisphere, a major disturbance propagated in all directions around the occulting disk. The C3 running difference images in Figure 6 provide an overview of this dramatic event as it appeared in the northeast quadrant (cropped to 15 $R_\odot$ on each side). The first two panels show the disturbance moving across the 4–15 $R_\odot$ field

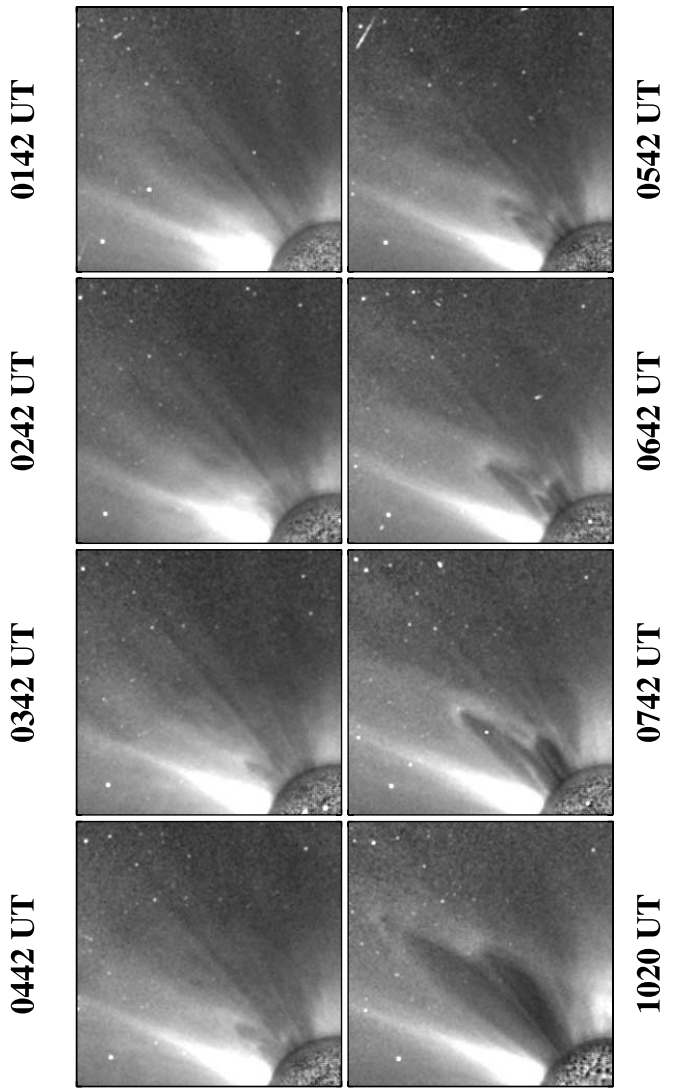

FIG. 7.—C3 minimum-subtracted images, corresponding to the difference images in Fig. 6 and showing the density depletions behind the individual outward components.

of view during 01:42–02:42 UT. By 02:42 UT, a small arch-shaped feature (*arrow*) has become visible behind the trailing edge of this wave. It is the first of several arches that form near 5 $R_\odot$ and then move outward to catch the previous ones. By 04:42 UT a second arch forms behind the first one, which has moved to about 6 $R_\odot$. Like all outward components seen in running difference images, these arches have the leading-white/trailing-black signatures of density enhancements. The second arch moves faster than the first and overtakes it by 06:42 UT when two new arches become visible near 5 $R_\odot$. These new arches move even more rapidly outward and begin to merge with the earlier ones at 08:18 UT to form a single, large, cusp-shaped loop, which is still visible at 10:20 UT when the sequence ends.

If these arches are really the outward components of in/out pairs, then minimum-subtracted images ought to show coronal depletions behind these outward components. The minimum-subtracted images in Figure 7 show the expected depletions, eventually merging into a single dark region.

Figure 8 shows running difference height/time maps for this event. The top panel refers to the 3 day interval 2004 January 18–20 and shows the gradually rising flow field for about 34 hr before it ended with the passage of the CME at 01:00 UT on January 20 and the subsequent formation of the in/out pairs. The bottom panel shows an expanded view of this action, beginning with a pair of widely spaced white tracks of the CME at 01:00 UT.

The scenario is essentially the same as that observed in Figure 7. The tracks of one or two slowly rising outward components emerge from the blurry pair of CME tracks at 01:00 UT. The track of another, faster outward component forms at about 04:00 UT and overtakes the slower of the first two tracks at 06:00 UT. Around 10:00 UT, the merged track is overtaken by a third, even steeper track, which separated from an inward track of pointed loops at 08:00 UT. By 10:00 UT, the height/time map shows little flow below 15 $R_\odot$, except for the remnants of these collapsing loops.

In Figure 9, the C2 running difference images show the northeast quadrant (6 $R_\odot$ on each side) during 07:31–12:30 UT, when the final outward components were separating from their inward counterparts. At 07:31 UT, the outward components are visible as they merge into a single cusp-shaped feature and separate from an apparent arcade of pointed loops (*arrow*). The remaining images show the collapse and progressive rounding of these loops.

In this paper, we have shown in/out pairs that formed spontaneously and in/out pairs that seem to have been triggered by the disturbance from a CME. However, we have also found cases in which a CME triggered a single in/out pair and other cases in which a sequence of pairs occurred spontaneously without the occurrence of a CME. But the common characteristic of all these in/out pairs is their location at the end of a gradually rising coronal structure.

2.4. *Events without Inward Components*

As mentioned above, some events have all of the properties of an in/out pair, except for an observed inward component. Figure 10 shows such an event on 2004 October 16–17. In the left panels, the running difference images show the weak signature of a slowly rising loop system at 06:30 UT and the strong signature of a much faster rising arch during 22:30–00:30 UT. The arch has the leading-white/trailing-black signature of a density enhancement. In the right panels, the minimum-subtracted images show this density enhancement and the depletion left behind it. Like the outward components of many in/out pairs, this "loop" has the corrugated shape of a helical flux rope whose legs remain attached to the Sun. The outward component looks so much like an eruptive prominence that we wonder whether it is prominence material carried up from the chromosphere and ionized, as we often observe for CMEs with a three-part structure (leading edge, trailing cavity, and central core), or whether it was produced in situ like the outward components of the ~160 observed in/out pairs. Of course, this leads to the related question of whether the trailing dark region is a rising streamer cavity or a new depletion created during the formation of an in/out pair below the occulting disk.

Figure 11 shows the corresponding height/time maps. Like the height/time maps of in/out pairs (cf. Figs. 3 and 5), these maps show about 32 hr of gradual expansion ending with the steep (330 km s^{-1}) upward track of an outward component. However, in this event, the outward component begins at the occulting disk and an inward component is not visible, again raising the question of whether this event may be an in/out pair that formed below the occulting disk.

Figures 12 and 13 provide another example, this time on 2003 April 12–13. In the left panels of Figure 12, the C2 running difference images show the familiar characteristics of an outward component: an arch-shaped density enhancement in the wake of a gradual expansion. In the right panels, the minimum-subtracted

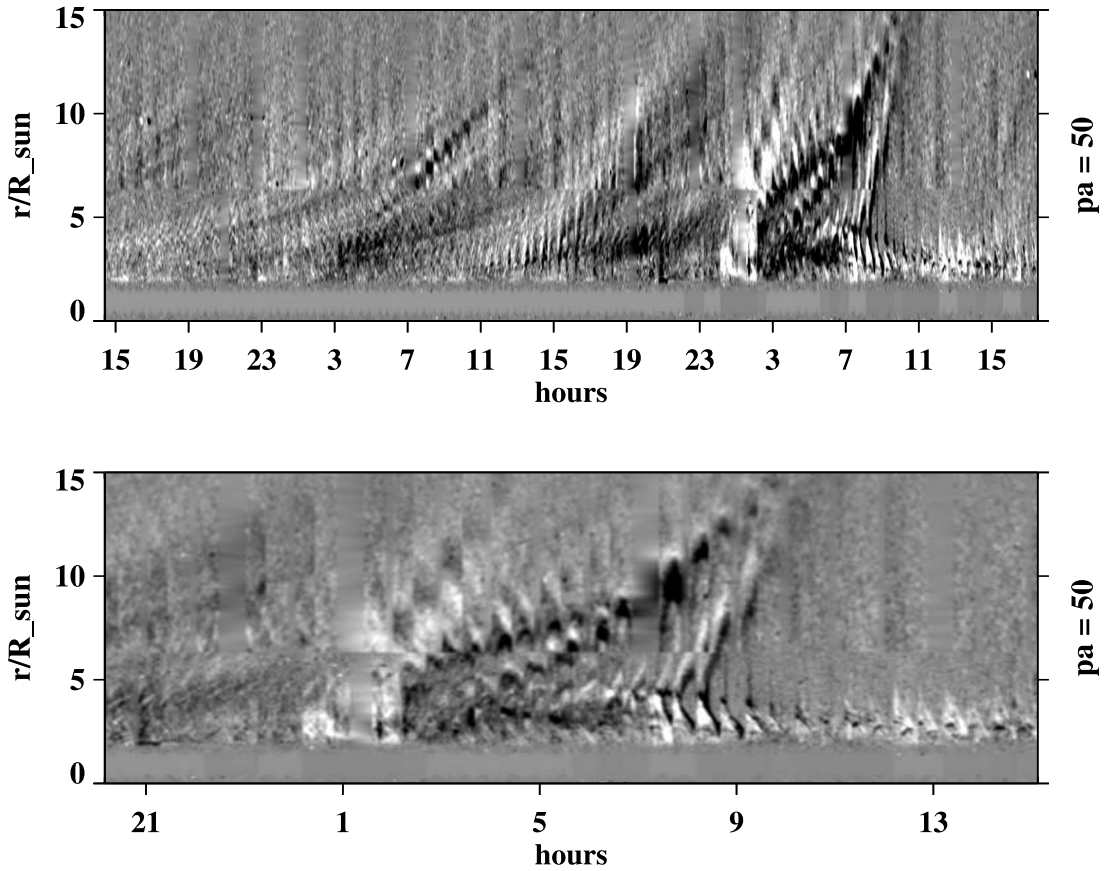

FIG. 8.—Running difference height/time maps, showing 1.5 days of gradual expansion prior to the occurrence of the halo CME and the triggered in/out pairs on January 20 (*top*) and an expanded view of the tracks that ended the expansion (*bottom*). The width of the slit used to make the height/time maps is 25 pixels here, but it is 17 pixels for the other figures in this paper. In the bottom panel, the final outward component tears away from pointed loops, which move inward and become rounder.

images show that this component was torn from a coronal streamer. Like the outward component on 2004 October 16–17 in Figure 10, this feature has a complicated fine structure, suggestive of a flux rope.

Unlike the October 16–17 images in Figure 10, these April 12–13 minimum-subtracted images show only a slight depletion behind the outward component. However, when the full complement of these images is viewed in a time-lapse movie, it shows a large depletion in the region between the legs of the arch in the running difference images. In the static images, this depletion is weakened by emission from the remaining streamer material along the line of sight. This overlapping intensity is greatly reduced in the running difference images and does not mask the visibility of the fast, bright outward component. However, the remaining streamer material does contribute to the fainter height/time tracks of the gradually rising feature, which extend slightly beyond the steeper ($\sim$400 km s^{-1}) and more intense track of the outward component, as shown in Figure 13. The streamer continued to be active at this location on April 14 when an in/out pair at 07:30 UT was followed by a small CME 2 hr later.

The top panel of Figure 13 shows that the track of the outward component did not begin at the occulting disk but instead started 0.5 $R_\odot$ above it at a distance of about 2.5 $R_\odot$ from Sun center. We suppose that this is a real effect and not entirely the result of the decreased resolution toward the occulting disk because the even fainter outward component shown in Figure 11 was visible right down to the occulting disk. This would mean that the outward component formed in the C2 field of view and did not simply emerge from a location below the occulting disk. Consequently, an inward component (if it occurred) must have narrowly missed detection just below the occulting disk.

The preceding examples raise the question of whether some in/out pairs may form below the occulting disk, where their inward components escape detection. Next, we examine histograms of the measured starting heights of 153 in/out pairs to see whether they are consistent with this hypothesis. We excluded about 60 additional events, such as those in Figures 10–13, for which inward components were not observed. Figure 14 contains histograms of the heights of the inward and outward components at the times when the inward component was first seen. It also contains histograms of the average of these two heights (providing an estimate of the common point of origin) and of their difference.

The distribution of inward starting heights, $r_{\rm in}$, is asymmetric with a sharp peak located below the 3.3 $R_\odot$ average value and a broad tail extending above this average. The steep falloff in the range 2.0–2.5 $R_\odot$ probably reflects the decreasing instrumental resolution toward the occulting disk and suggests that the distribution of all in/out pairs (unobscured by the occulting disk) would peak even closer to the Sun. By comparison, the distribution of outward starting heights, $r_{\rm out}$, is more symmetric and broadly peaked around its average value of 5.3 $R_\odot$. In particular, it is not the simple shift of the inward distribution that one would obtain if all of the starting separations, $r_{\rm out} - r_{\rm in}$, were the same. This implies that the distribution of starting separations must also be broad, as one can readily verify in the bottom right panel. Here the distribution of starting separations ranges from 1 to 3 $R_\odot$ and has a peak at 2 $R_\odot$. The breadth of this distribution is caused by temporal sampling of the LASCO observations, but the lower

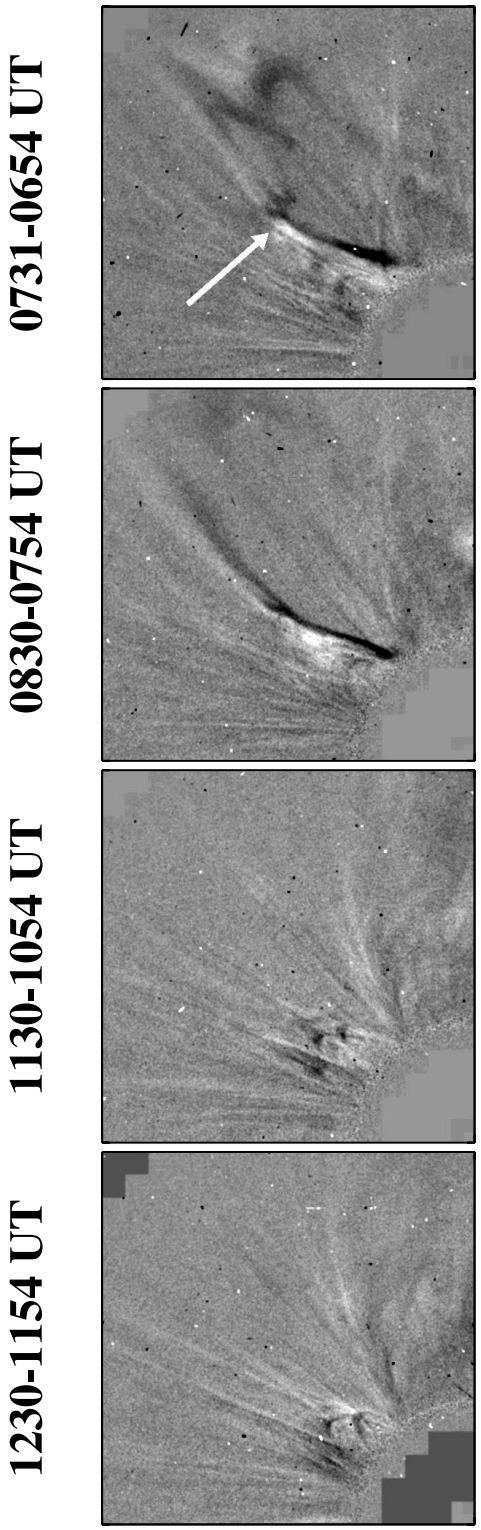

FIG. 9.—C2 running difference images on January 20, showing pointed loops detaching from their outgoing counterparts and becoming rounder as they collapse.

limit at 1 $R_\odot$ is a real effect, probably indicating that these features are exceedingly faint when they first appear. In the bottom left panel, the distribution of "extrapolated" starting heights, $(r_{in} + r_{out})/2$, is centered at an average value of 4.3 $R_\odot$. Its lower limit near 3 $R_\odot$ reflects the instrumental cutoff of 2.0–2.5 $R_\odot$ for the inward components plus the observed separation limit of about 1.0 $R_\odot$.

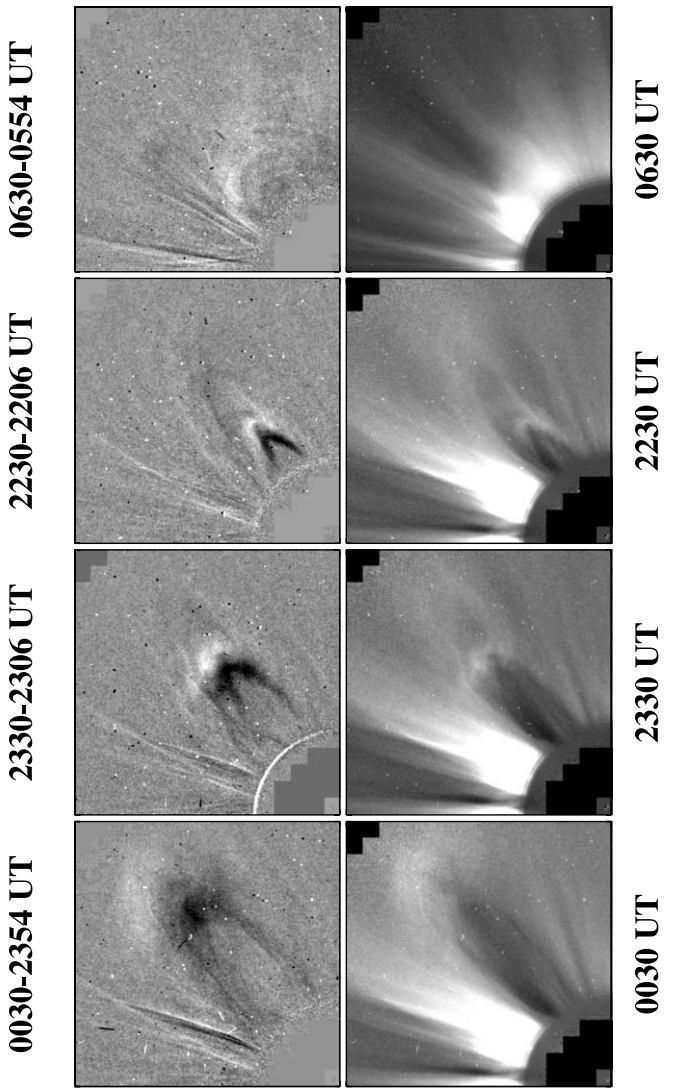

FIG. 10.—C2 running difference (*left*) and minimum-subtracted (*right*) images on 2004 October 16–17, showing an arch-shaped eruption at the end of an interval of coronal expansion. In the minimum-subtracted images, the arch develops a corrugated structure, similar to that of an eruptive prominence or helical magnetic flux rope.

It is plausible that the gradually expanding coronal structures indicate the rising loops of a growing magnetic field and that the in/out pairs are signatures of magnetic field line reconnection when the field stops growing and the detached field is carried away. In this case, the height of the reconnection might depend on a property of the expansion, such as its strength or size, so that "stronger events" reconnect closer to the Sun and "weaker events" reconnect farther out in the corona. In fact, our 60 events without inward components did tend to be larger than the events with observed inward components. (For example, 50% of the events without visible inward components had angular spans greater than 50°, which was the upper limit of the angular spans of the observed in/out pairs.)

Figure 15 shows one of these large events on 2004 February 13. In the left panels, the running difference images show a broad feature rising slowly across the northern hemisphere. Its disruption begins when a small dark arch emerges in the northwest and eventually spreads eastward to span the entire northern hemisphere. No inward component is visible. In the right panels, the minimum-subtracted images show the disruption of a coronal

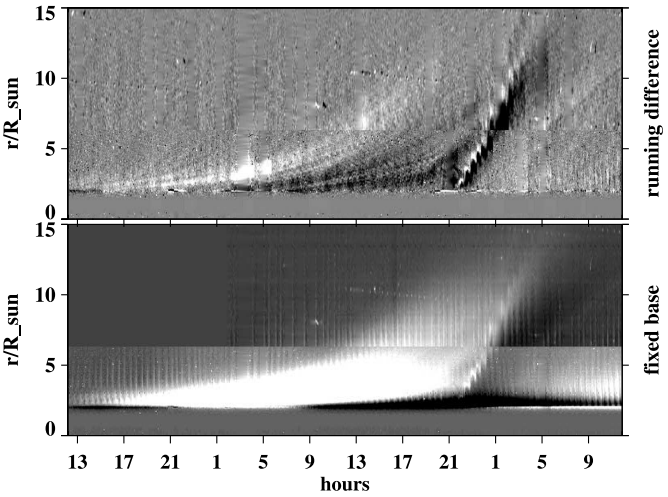

FIG. 11.—Height/time maps of the event in Fig. 10. A 1–2 day interval of gradual expansion ends with the occurrence of a steep outward component, which extends all the way to the occulting disk, but no inward component is visible. This might have been an in/out pair that originated below the occulting disk. The position angle is 35°.

streamer in the northwest and the formation of a depleted region behind the expanding loop. Figure 16 contains height/time maps obtained at three different position angles across the event. They show about 16 hr of slow expansion, terminated by a faster (250 km s^{-1}) depletion, but no evidence of an inward component. We suppose that this event has a slower projected speed than the previous, smaller events because it is more inclined out of the sky plane, like a halo CME.

In selecting the events of this section, we considered properties that are similar to those of in/out pairs such as the prior interval of gradual expansion ending with a sudden outward ejection. We tried to avoid events that had the traditional three-part structure (leading edge, trailing cavity, and central core) of CMEs. Because in/out pairs signify the end of gradually accelerating outflows, we have thought of them as CME-ending events, but not as CMEs themselves. In Paper I, we referred to them as "failed CMEs." Now, it is clear that all of these events involve the disruption of coronal streamers and that some of them (such as the 2004 February 13 event in Fig. 15) are streamer blowout CMEs observed face on.

Streamer blowout CMEs involve the gradual brightening and sudden eruption of coronal streamers and often have characteristic "bugle-like" signatures in Carrington maps of coronal intensity (Howard et al. 1985; Hundhausen 1993; Vourlidas et al. 2002 and references therein). Consequently, in Figure 17 we show Carrington maps of coronal intensity at 3 $R_\odot$ for the three events of this section. In the top panel, an east-limb map during Carrington rotation 2022 shows a vertical feature near 200° longitude, corresponding to the event of 2004 October 16. The broad latitudinal extent of this feature is similar to those we have found for other such events but differs from the bugle-like appearance of some streamer eruptions. In the middle panel, an east-limb map during rotation 2002 shows the end of a streamer-related feature near 310° longitude, corresponding to the event of 2003 April 12. This feature has the bugle-like signature of a streamer eruption.

In the bottom panel, a west-limb map of coronal intensity during rotation 2012 shows the disruption of a streamer near 50° longitude, corresponding to the event on 2004 February 13. This feature extends to the north pole and continues back down to lower latitudes near 210° longitude on the east-limb map of rotation 2013 (not shown here). By comparing these maps with Carrington maps

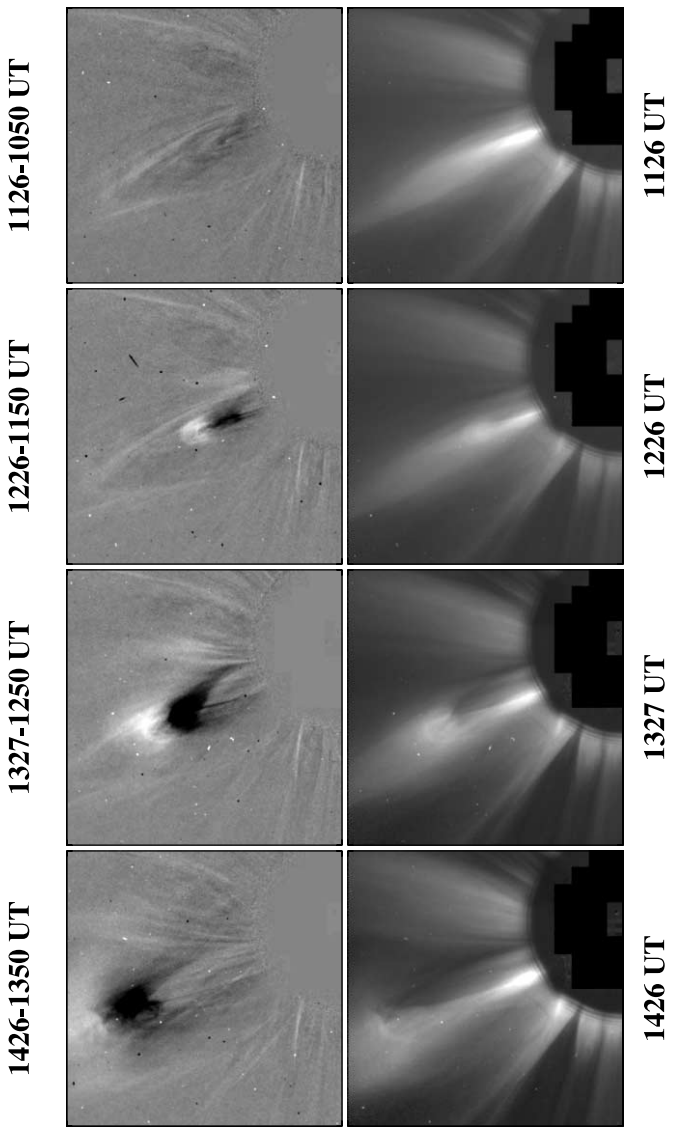

FIG. 12.—C2 running difference images (*left*) and minimum-subtracted images (*right*) of the southeast quadrant of the corona on 2003 April 13, showing a streamer disruption without a visible inward component.

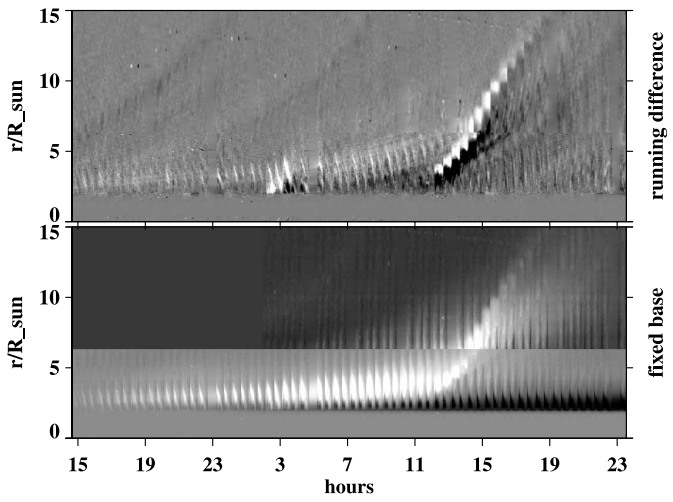

FIG. 13.—Height/time maps of the streamer disruption event in Fig. 12. The outward component forms about 0.5 $R_\odot$ above the occulting disk, but no inward component is visible. The position angle is 115°.

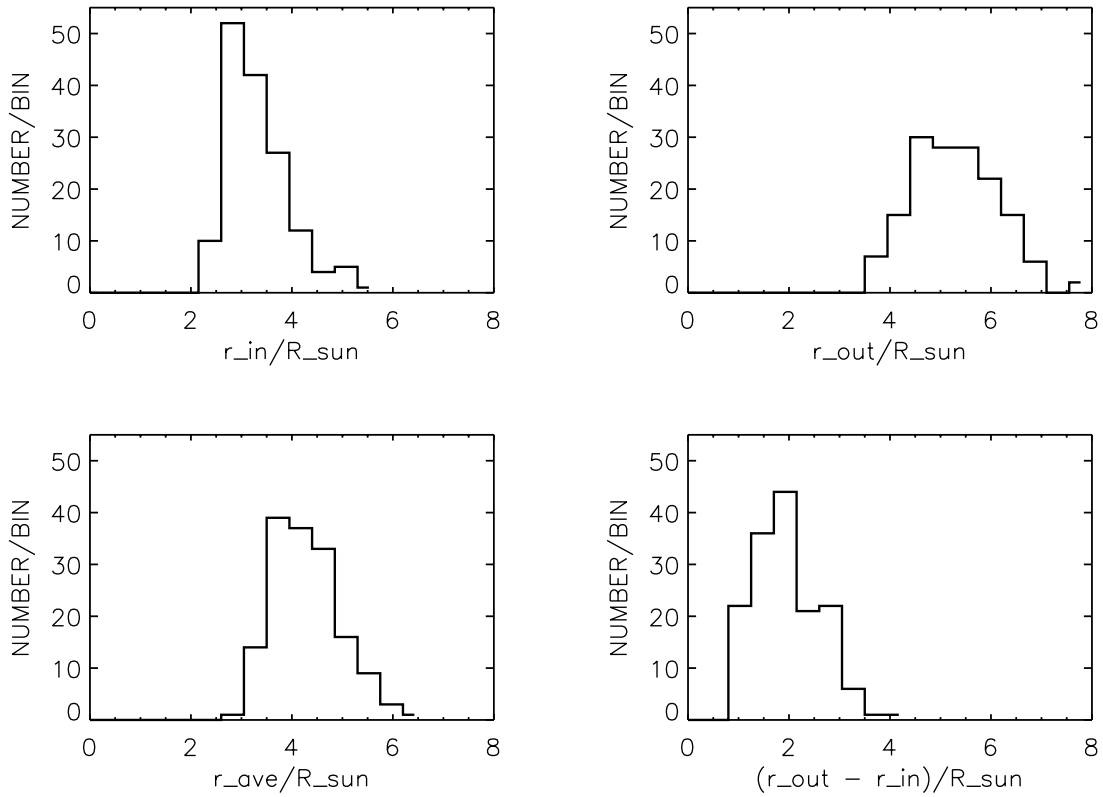

FIG. 14.—Histograms of the starting heights of 153 observed in/out pairs, showing the heights of the inward components (*top left*) and outward components (*top right*), their averages (*bottom left*), and their differences (*bottom right*). The bin size is 0.45 for each distribution. Relative to the other distributions, the distribution of starting heights for the inward components is strongly peaked and skewed to the right. The sudden drop toward the occulting disk at 2.0 $R_\odot$ is instrumental and suggests that many unobserved pair formations may have occurred closer to the Sun.

of the photospheric field and its coronal extension, we found that the Sun's field had a prominent two-sector structure, corresponding to a dipole field whose axis was tipped slightly toward Earth on February 13. Thus, we suppose that this large eruption started at the west limb and spread for about 160° along the northern-hemisphere streamer belt, which was then located on the back side of the Sun.

3. SUMMARY AND DISCUSSION

In the previous section, we describe the results of examining a collection of more than 160 in/out pairs and 60 similar events whose inward components, if they occurred, were masked by the occulting disk. We found that the inward and outward components occur along the leading and trailing edges of depletions that form when slowly expanding coronal structures finally separate from the Sun.

However, we also found that the separation is not complete. The legs of the arch-shaped outward component extend back toward the occulting disk and apparently remain connected to the Sun. This is what we would expect if the outward component were a helical flux rope, created when the loops of an expanding arcade reconnect with each other in the manner originally suggested by Gosling (1990). As discussed in Paper I, the outward component often has a corrugated structure that is consistent with the helical configuration of a magnetic flux rope, and the inward component occasionally resolves into a system of collapsing loops.

The final separation of the streamer material often occurs spontaneously without an obvious cause. However, almost equally often, the separation seems to be triggered by the passage of a wavelike disturbance from a large, high-speed CME. This suggests that the disturbance may push the reconnecting field lines together sooner than would otherwise happen and raises the question of what determines the time and place of the reconnection when there is no CME.

The events without visible inward components tend to be bigger than those with inward components, but otherwise they have similar properties. The gradual expansion involves the same marble-like fine structure, the same 20 km s^{-1} speed, and the same 1–2 day duration. The expansion ends as a collection of loops tears away from the streamer and acquires a corrugated, prominence-like structure similar to that of a helical magnetic flux rope. The largest events have characteristic bugle-like signatures in Carrington maps of coronal intensity and are probably streamer blowout CMEs (Howard et al. 1985; Hundhausen 1993; Sheeley et al. 1997; Vourlidas et al. 2002). Thus, in/out pairs and streamer blowout CMEs seem to be part of the same broad class of streamer eruption events, differing in their strengths, sizes, and coronal heights of formation. Many of the large events without inward components extend over the poles (such as the 2004 February 13 event in Fig. 15) and therefore are probably streamer blowout CMEs seen face on.

An advantage of the in/out pairs is that they show the separation that marks the end of the coronal expansion, rather than just the ejection of the outward component. Consequently, for these events, we know that the corrugated outward components are created in the corona during the separation and are not simply carried up from the chromosphere. This suggests that the eruptive prominences that accompany some streamer blowout CMEs may acquire their helical shapes during a similar reconnection process that occurs much closer to the Sun.

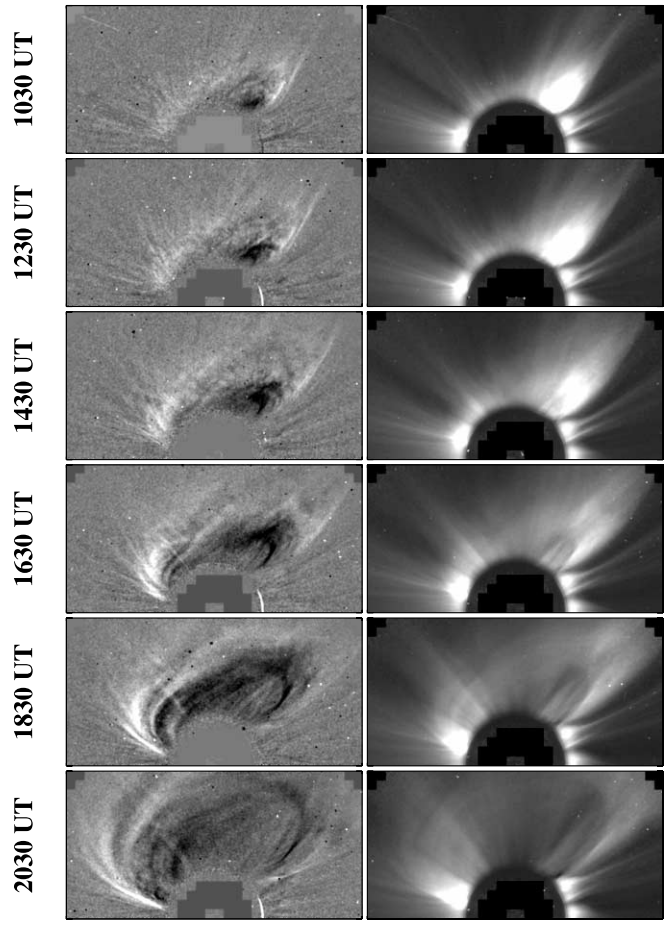

FIG. 15.—C2 running difference images (*left*) and minimum-subtracted images (*right*), showing the gradual expansion and eventual disruption of a coronal structure on 2004 February 13. The evolution begins with the coronal streamer in the northwest (*upper right*), but eventually spreads along the streamer belt to span the entire northern hemisphere.

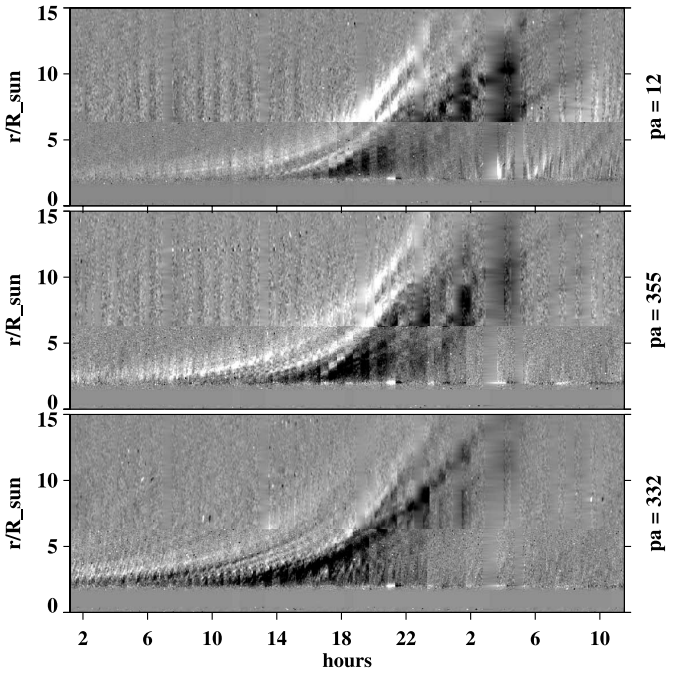

FIG. 16.—Running difference height/time maps obtained at three radial positions in the 2004 February 13 event of Fig. 15, comparing the evolution in the northeast (*top*), north (*middle*), and northwest (*bottom*) directions.

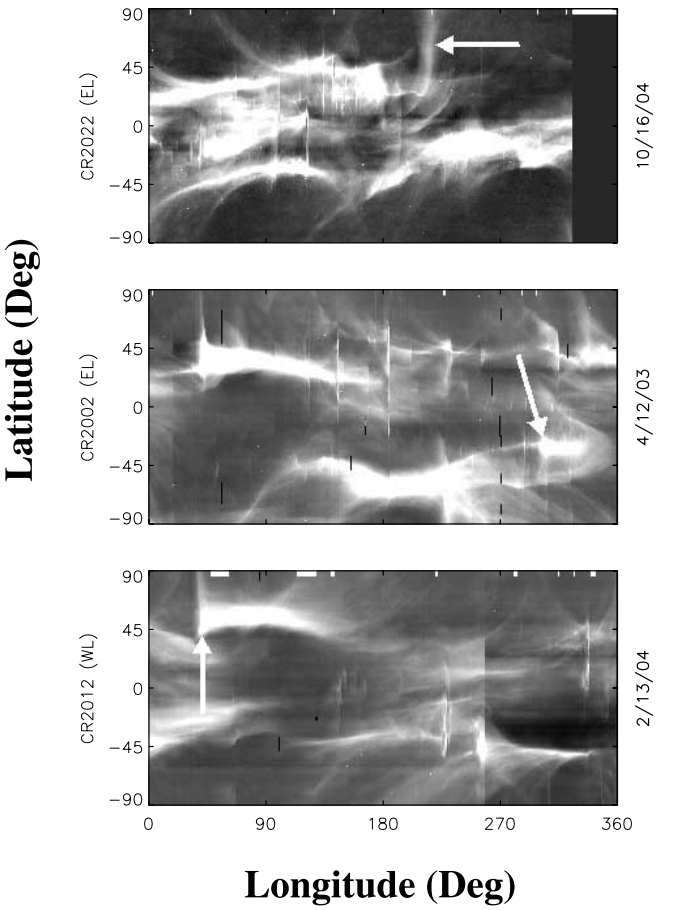

FIG. 17.—Carrington maps of white-light coronal intensity at 3 $R_\odot$. The arrows indicate events without inward components on 2004 October 16 (*top*), 2003 April 12 (*middle*), and 2004 February 13 (*bottom*), which we have shown in Figs. 10, 12, and 14, respectively. The latter two events have the characteristic signatures of streamer blowout CMEs.

As mentioned above, we suppose that the slowly rising coronal structures indicate closed loops of a growing magnetic field, produced either by the emergence of new flux at the photosphere or by the separation of the footpoints of a magnetic arcade by photospheric motions or reconnection between adjacent loop systems. In fact, running differences between closely timed images sometimes show a crisscross pattern resembling the overlapping loops of a magnetic arcade seen in projection along the line of sight. Evidently, the LASCO observations are revealing the transient process that occurs when the field stops growing—namely, the reconnection of the fields in the rising arcade and the separation of the newly reconnected parts. This transient behavior is not included in a sequence of potential fields, whose rising loops become stationary when the field stops growing.

However, a similar transient behavior is obtained when one retains the time-dependent terms in Maxwell's equations and calculates the evolution of a vacuum dipole field when its source current is gradually ramped up from one stationary value to another. This change produces an outgoing wave whose leading edge enhances the background field and whose trailing edge reduces it (unpublished calculations by N. R. Sheeley 1997, private communication). The result is a bulge at the front of the transient and a pinch-off at the rear where the outgoing wave separates from the strengthened dipole field left in its wake. In this case, the separation is an unmistakable consequence of ending the growth and

provides strong motivation for interpreting the formation of in/out pairs in terms of a similar "edge effect."

We imagine that the process occurs in two phases. During the steady state phase, the loops rise slowly as the field grows. Eventually, these slowly rising loops are far enough from the Sun that their magnetic tension cannot hold them back, and they accelerate outward with the solar wind. This gradual expansion and subsequent acceleration continues as long as the growth continues and is responsible for carrying closed field lines out into the heliosphere without reconnection. However, as soon as the growth stops (or slows), new loops do not rise up to replace the older ones whose tops have been carried away (or else the new loops rise up more slowly). Consequently, the legs of the older, highly stretched loops are no longer held apart and move toward each other to form a thinning plasma sheet. Eventually, these oppositely directed field lines meet and reconnect. Because the reconnection occurs in three dimensions, it produces an outgoing helical flux rope whose ends remain attached to the Sun (rather than the detached rings obtained for an axisymmetric field) and an ingoing system of collapsing loops. In effect, by decreasing the rate at which new loops rise up to replace the old ones, the Sun creates space for reconnection between the stretched loops of the rising arcade. Thus, the thinning plasma sheet is a consequence of this nonsteady source of magnetic loops (or possibly a nonsteady flow that carries them away) and is analogous to the rarefaction that forms in the wake of a high-speed solar wind stream. Further discussion of this idea is contained in the Appendix.

The gradual expansion that precedes all of these streamer detachment events (from in/out pairs to streamer blowout CMEs) is characterized by a long (1–2 day) interval of very slow ($\sim$20 km s^{-1}) upward motion, culminating in an acceleration to solar wind speeds of several hundred kilometers per second. It differs from the streamer detachment itself in which an upward and downward component are suddenly released when the era of gradual expansion is over. In the gradual phase, one can think of the height/time track as being composed of three segments: an initial linear segment (where the speed is $\sim$20 km s^{-1} but constant) followed by a curved segment (where an acceleration of about 10 m s^{-2} increases the speed) and a final linear segment (where the speed is 300–400 km s^{-1}, again constant). In effect, the closed loops rise slowly upward until they reach the acceleration region and are carried away in the solar wind. In the streamer detachment phase, the nonsteady condition causes the field lines to reconnect, and the oppositely directed components move rapidly apart, initially at constant speed, but then decelerating as they encounter dense plasma ahead of them. We will present our measurements and analysis of these motions in a future paper.

We previously speculated (Sheeley & Wang 2002) that in/out pairs are face-on views of streamer disconnection events like those we observed at sunspot minimum and during the rising phase of the sunspot cycle (Wang et al. 1999). We argued that the speeds and two-part structures are similar, and we noted that the depleted region left between the inward and outward components matches the thinning portion of the pinched streamer. In addition, we mentioned that the disconnection events disappeared around sunspot maximum when the in/out pairs first appeared, as if they were the same kinds of events seen from the different perspectives provided at sunspot minimum and maximum. The much larger statistical sample provided by our new study supports this conclusion. The similar geometries and kinetic properties of in/out pairs and streamer disconnection events leaves little doubt that they are the same.

In that previous paper, we also described a type of inflow ("falling curtains") that began with a gradually rising coronal structure and ended with the sudden appearance of a collapsing loop system in the C2 field of view (Sheeley & Wang 2002). Because the loops appeared suddenly, we speculated that they may have formed when the neighboring field lines of a rising magnetic arcade reconnected in a "chain reaction" to produce a single, large rising loop and several smaller collapsing loops beneath it, similar to those shown in Figure 3*a* of Gosling et al. (1995). In our present study, we found that virtually all of these falling curtains were accompanied by outward components in the C3 field of view. We conclude that those falling curtains are in/out pairs for which the outward component was not strongly visible until it entered the C3 field of view.

It would be interesting to relate these streamer eruptions to the magnetic fields and plasma structures back at the Sun and farther out in the heliosphere. For the larger events, we expect to find growing bipolar magnetic regions or sheared neutral lines with eruptive prominences, as well as changes in the boundaries of coronal holes. Of course, magnetic clouds are obvious candidates for the in situ signatures of the outward components. However, in a previous comparison between coronal observations obtained from the Solwind instrument aboard the Earth-orbiting *P78-1* satellite and interplanetary measurements obtained with the *Helios 1* spacecraft, located 90° from the Sun-Earth line, we found a convincing association between a magnetic cloud and a large CME, which was apparently not a streamer blowout (Burlaga et al. 1982). On the other hand, we also found a clear association between a relatively slow (270 km s^{-1}), streamer blowout CME on 1979 May 27 and a piston-driven shock at *Helios 1* (Sheeley et al. 1983, 1985), as if the disturbance accelerated to higher speeds beyond the 10 $R_\odot$ limit of the Solwind coronagraph. Thus, a search for the solar and interplanetary signatures of these streamer eruption events may provide some interesting surprises.

We are grateful to the *SOHO* LASCO team for help, encouragement, and solar observations. In particular, N. B. Rich and K. Battams provided the Carrington maps of coronal intensity used in Figure 17, and A. Vourlidas contributed useful information about streamer blowout CMEs. We are also grateful to our summer students J. Biersteker (Harvard College) and C. Bogdan (Thomas Jefferson High School of Science and Technology), who assisted with the quantitative analysis of our height/time measurements. Financial support was obtained from NASA and the Office of Naval Research.

APPENDIX

A CURRENT-SHEET MODEL OF STREAMER DETACHMENT

In § 3, we interpret LASCO observations of streamer detachments in terms of an assumed variation in the source rate of emerging loops. When the source rate is constant, loops rise up into the acceleration region to replace those that have been carried away in the solar wind. Consequently, long closed loops extend outward into the solar wind without pinching off. Only when the source rate decreases (or falls to zero) do new loops fail to replace those that were carried away and allow the legs of the older loops to pinch together to form an outgoing flux rope.

Next, we consider a simple model to describe the magnetic field line topology that results from such a process. This model is analogous to the time-dependent solution for a growing vacuum dipole field (unpublished calculations by N. R. Sheeley 1997, private communication), whose evolution involves the ejection of a toroidal ring of displacement current. The magnetic field of this "current" has closed poloidal contours whose leading and trailing edges are directed along and opposite the field lines of the underlying dipole. Consequently, this transient causes a bulge as it enters the background field and a pinch-off as it leaves the stronger dipole in its wake. The gist of our model is to replace the displacement current of this time-varying vacuum field with a real electric current and to combine the resulting magnetic field with the field of a fixed dipole.

We do this by considering a vector potential, $\boldsymbol{A}$, whose only component in the (r, θ, ϕ) spherical coordinate system is

$$A_\phi = f(r) \sin^n \theta, \tag{A1}$$

where $f(r)$ is a function to be selected and n is a positive integer that we make large to compress the resulting current distribution into a narrow sheet near the equator. We refer to the field of this "flat" current as the "current-sheet field," but it is really only a perturbation on the field of the Sun's current sheet, which is not included in this simple model. This vector potential generates a poloidal magnetic field $\boldsymbol{B}$ whose components are

$$B_r = (n+1)\frac{f(r)}{r} \sin^{n-1} \theta \cos \theta, \tag{A2a}$$

$$B_\theta = -\left[f'(r) + \frac{f(r)}{r}\right] \sin^n \theta. \tag{A2b}$$

The solenoidal condition $\nabla \cdot \boldsymbol{B} = 0$ is automatically valid because $\boldsymbol{B} = \nabla \times \boldsymbol{A}$. However, in general, the curl-free condition $\nabla \times \boldsymbol{B} = 0$ is not valid. Using the components of $\boldsymbol{B}$ given by equations (A2a) and (A2b), we find a single component of $\nabla \times \boldsymbol{B}$ given by

$$(\nabla \times \boldsymbol{B})_\phi = -\left[f'' + \left(\frac{2}{r}\right)f' - n(n+1)\frac{f}{r^2}\right] \sin^n \theta - \left(n^2 - 1\right)\left(\frac{f}{r^2}\right) \sin^{n-2} \theta. \tag{A3}$$

This curl does vanish for a dipole field, which has $n = 1$, $f(r) = r$ (inside $r = 1$), and $f(r) = r^{-2}$ (outside $r = 1$), but our objective is to construct a field whose curl does not vanish.

Because the field is axisymmetric, its field lines are contours of constant flux given by

$$\Phi = 2\pi r^2 \int_0^\theta B_r \sin \theta \, d\theta = 2\pi r \sin \theta A_\phi. \tag{A4}$$

Using the vector potential A_ϕ in equation (A1) and replacing π with the flux Φ_1 through a unit sphere, we obtain

$$\frac{\Phi}{\Phi_1} = F(r) \sin^{n+1} \theta, \tag{A5}$$

where we have made the substitution $F(r) = 2rf(r)$.

Our next objective is to define $F(r)$ to give poloidal contours inside a limited region of space. We consider a function of the form

$$F(r) = \frac{(r - r_0)(r_1 - r)}{\Delta^2}, \tag{A6}$$

where $r_0 < r_1$ and $\Delta = (r_1 - r_0)/2$. In this case, F ranges from 0 at the left end of the interval (r_0, r_1) to 1 at the center (where $r = r_c = r_0 + \Delta = r_1 - \Delta$) and back to 0 again at the right end. Thus, the field lines are closed contours that surround the midpoint, r_c, and are given by values of constant flux Φ/Φ_1 ranging from 0 at the edge (where $r = r_0$ and $r = r_1$) to 1 at the center (where $r = r_c$).

Note that with this definition of F, the field at the equator (where $\theta = \pi/2$) is

$$B_\theta = -\left(f' + \frac{f}{r}\right) = -\frac{F'}{2r} = \left(\frac{1}{\Delta^2}\right)\left(\frac{r - r_c}{r}\right), \tag{A7}$$

which ranges from $-1/(r\Delta)$ at the left end of (r_0, r_1), to 0 at the center, to $+1/(r\Delta)$ at the right end. This means that the field lines run clockwise about the center of the current sheet and that the maximum strength of this field decreases with radial distance as r^{-1}. By comparison, the dipole field,

$$B_r = B_0 r^{-3} \cos \theta, \tag{A8a}$$

$$B_\theta = \left(\frac{B_0}{2}\right) r^{-3} \sin \theta, \tag{A8b}$$

has a radial dependence at the equator given by $B_\theta = (B_0/2)r^{-3}$. Thus, at large distances from the origin, the current-sheet field is dominant, and at small distances the dipole field is dominant.

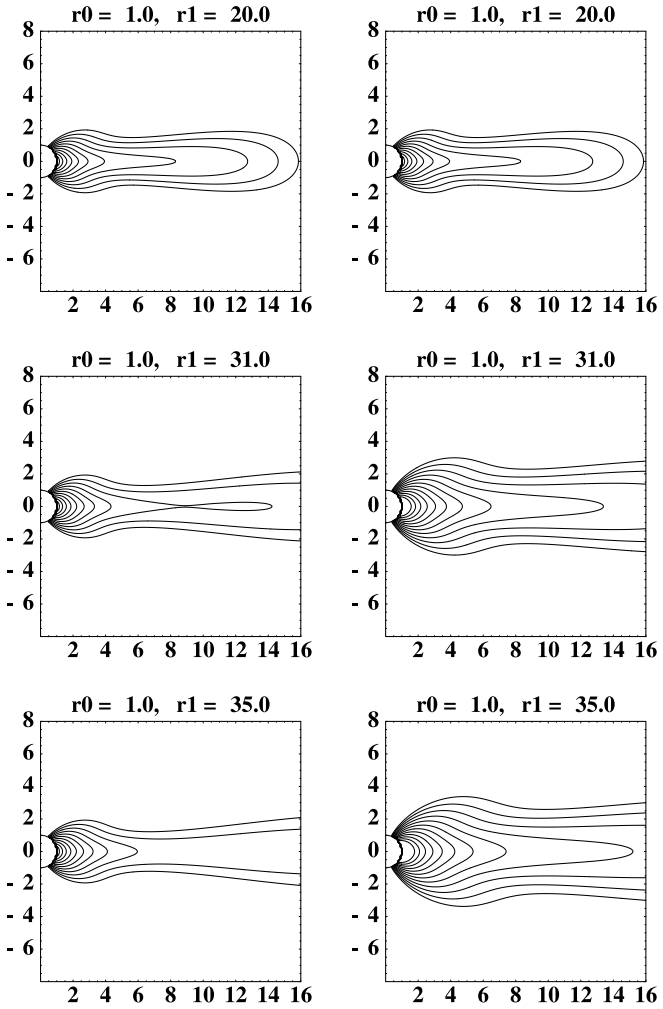

FIG. 18.—Cartoon illustrating the field line evolution without (*left*) and with (*right*) replenishment from below. When the expanding field lines are dragged outward without replacement from below (*left*), their legs pinch together and reconnect, limiting the amount of open flux at the Sun. However, when new loops rise up to replace the expanding field lines (*right*), they prevent reconnection and allow the amount of open flux to increase. (See the Appendix for details.)

We can determine where the reconnection begins by assigning a strength B_1 to the current-sheet field (analogous to B_0 for the dipole field in eqs. [A8a] and [A8b]) and setting the combined equatorial field equal to 0:

$$\left(\frac{B_0}{2}\right)\left(\frac{1}{r^3}\right)+\left(\frac{B_1}{\Delta^2}\right)\left(\frac{r-r_c}{r}\right)=0. \tag{A9}$$

This reduces to a cubic equation for r,

$$r^3-r_c r^2+\frac{\Delta^2}{2\alpha}=0, \tag{A10}$$

where $\alpha = B_1/B_0$. If r_c is sufficiently large, this equation will have two positive roots (giving the locations of an X-type and an O-type neutral point). However, if r_c is too small, then there will be no positive roots and reconnection will not occur. This special value of r_c occurs when these two roots are equal and is obtained by setting the derivative of this cubic polynomial equal to zero and substituting the resulting value of r back into equation (A10). The result is

$$r=\left(\frac{\Delta^2}{\alpha}\right)^{1/3}, \tag{A11a}$$

$$r_c=\left(\frac{3}{2}\right)\left(\frac{\Delta^2}{\alpha}\right)^{1/3}. \tag{A11b}$$

Thus, the reconnection begins close to the origin if the current-sheet field is relatively strong compared to the background field and far from the origin if the current-sheet field is relatively weak. A similar argument may apply to the heights of formation of in/out pairs.

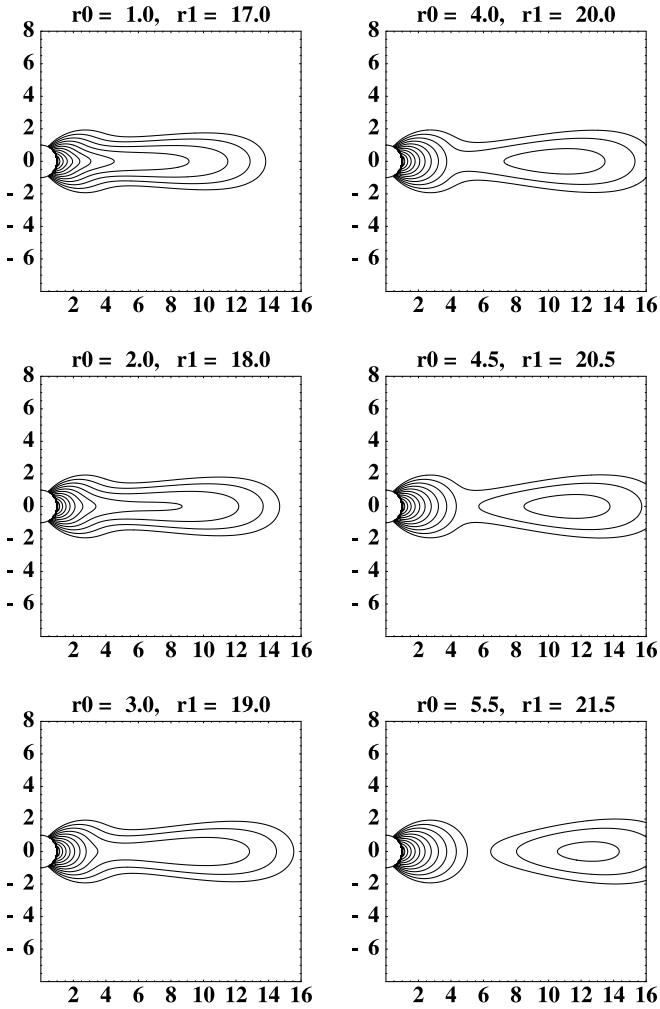

FIG. 19.—Cartoon illustrating the streamer detachment that occurs when the interval of loop replacement is over. The longer loops continue outward, while the shorter loops contract back toward the Sun, leaving space for the field lines to reconnect and a flux rope to be ejected from the Sun. (See the Appendix for details.)

In any case, it is important to recognize that there will be no reconnection if r_c is less than the value given by equation (A11b). Recalling that Δ and r_c are determined by r_0 and r_1, we can write the reconnection inequality as a condition on α, the strength of the current-sheet field relative to that of the dipole. Thus, reconnection will not occur if

$$\alpha < \frac{27}{8}\left(\frac{1}{\Delta}\right)\left(\frac{\Delta}{\Delta + r_0}\right)^3. \tag{A12}$$

If $r_0 \ll r_1$ then this reduces to $\alpha\Delta < 3.375$ or, equivalently, $\alpha r_1 < 6.75$. In particular, if the expanding coronal gas stretches the field lines out into a growing current sheet with r_0 fixed near 1 and r_1 becoming progressively larger, then αr_1 will eventually exceed 6.75, and the legs of the extended field lines will reconnect. However, the reconnection does not occur if α decreases during the expansion, so its product with r_1 remains less than 6.75. If the strength B_1 of the current-sheet field remains constant, then the strength B_0 of the dipole must increase. In effect, the growing dipole replaces the field that is stretched out and prevents the reconnection.

This behavior is illustrated in Figure 18, which was created by drawing contours of constant flux Φ given by

$$\Phi = \Phi_0 \frac{\sin^2\theta}{r} + \Phi_1 F(r) \sin^{n+1}\theta, \tag{A13}$$

where Φ_0 and Φ_1 are the dipole flux and current-sheet flux, respectively, through unit spheres as given by $\Phi_0 = \pi B_0$ and $\Phi_1 = \pi B_1$. For the left panels, we chose $\Phi_0 = 1$, $\Phi_1 = 0.2$, and $r_0 = 1$ and let r_1 increase from 20 to 31, and finally to 35. The index n was assigned a relatively large value of 41 to keep the current confined close to the equator. These stretched field lines have begun to reconnect by the time that the right edge of the current sheet reaches $r_1 = 31$. (Eqs. [A11a] and [A11b] give $r_1 = 28.3$ and $r = 9.8$ as the birthplace of the neutral points.) For the right panels, we again chose $\Phi_1 = 0.2$ but let Φ_0 increase to keep $\alpha r_1 = 4$. Thus, for the three right panels, Φ_0 had values of 1, 1.55, and 1.75 from top to bottom, respectively. As one can see, the increase of flux in the dipole field prevented reconnection of the expanding fields.

Of course, this increase in dipole strength is part of our simulation, and on the real Sun the increase may have several possible origins, including the emergence of new flux, the separation of the footpoints of an arcade by photospheric motions, or the reconnection between

adjacent loop systems in the lower corona. Or it may be caused by variations in the flow speed that drags the field lines outward. The essential point is that there must be an increase in the rate at which flux is transported outward through the corona. We suppose that this happens during the gradual phase of in/out pairs and streamer blowout CMEs.

Figure 19 shows the field lines when the current sheet is assigned a constant width, $r_1 - r_0 = 16$, but is allowed to move away from the origin. As in Figure 18, we chose values of $\Phi_0 = 1$, $\Phi_1 = 0.2$, and $n = 41$. Reconnection occurs much sooner in this case, the shorter loops retracting by the time that $r_1 = 19$ and leaving space for the legs of the longer loops to move together and reconnect. (Eqs. [A11a] and [A11b] give $r_1 = 19.5$ and $r = 6.8$ as the start of the pinch-off.) All three of the longer loops have detached by the time that $r_1 = 21.5$. This rapid separation seems analogous to the end phase of an in/out pair or a streamer blowout CME whose pinch-offs send ejections outward at much higher speed than the loops that preceded them during the gradual phase. In addition, the Sun's field is not axisymmetric in general, so the reconnection occurs in three dimensions. Consequently, the outward ejections are helical flux ropes whose distant ends remain connected to the Sun, rather than the detached loops shown in Figures 18 and 19.

In summary, we think of streamer detachments as the Sun's way of adjusting to variations in the rate of rising loops. When the rate increases, loops are dragged out to inflate the current sheet. When the increase stops, the legs of the stretched loops reconnect, sending flux ropes outward and collapsing loops inward, and forming the new state of the coronal streamer. It is plausible that raining inflows are manifestations of the adjustments that take place when there are decreases in the rate at which loops are carried outward from the Sun.

REFERENCES

Asai, A., Yokoyama, T., Shimojo, M., & Shibata, K. 2004, ApJ, 605, L77

Burlaga, L. F., Klein, L., Sheeley, N. R., Michels, D. J., Howard, R. A., Koomen, M. J., Schwenn, R., & Rosenbauer, H. 1982, Geophys. Res. Lett., 9, 1317

Gallagher, P. T., Dennis, B. R., Krucker, S., Schwartz, R. A., & Tolbert, A. K. 2002, Sol. Phys., 210, 341

Gosling, J. T. 1990, in Physics of Magnetic Flux Ropes, ed. C. T. Russell, E. R. Priest, & L.-C. Lee (Washington: American Geophysical Union), 343

Gosling, J. T., Birn, J., & Hesse, M. 1995, Geophys. Res. Lett., 22, 869

Howard, R. A., Sheeley, N. R., Michels, D. J., & Koomen, M. J. 1985, J. Geophys. Res., 90, 8173

Hundhausen, A. J. 1993, J. Geophys. Res., 98, 13177

Innes, D. E., McKenzie, D. E., & Wang, T. 2003a, Sol. Phys., 217, 247

———. 2003b, Sol. Phys., 217, 267

McKenzie, D. E. 2000, Sol. Phys., 195, 381

McKenzie, D. E., & Hudson, H. S. 1999, ApJ, 519, L93

Sheeley, N. R., Howard, R. A., Koomen, M. J., Michels, D. J., Schwenn, R., Muhlhauser, K. H., & Rosenbauer, H. 1983, in Solar Wind Five, ed. M. Neugebauer (Washington: NASA), 693

Sheeley, N. R., Howard, R. A., Michels, D. J., Koomen, M. J., Schwenn, R., Muehlhaeuser, K. H., & Rosenbauer, H. 1985, J. Geophys. Res., 90, 163

Sheeley, N. R., Knudson, T. N., & Wang, Y.-M. 2001, ApJ, 546, L131

Sheeley, N. R., Walters, J. H., Wang, Y.-M., & Howard, R. A. 1999, J. Geophys. Res., 104, 24739

Sheeley, N. R., & Wang, Y.-M. 2001, ApJ, 562, L107

———. 2002, ApJ, 579, 874

Sheeley, N. R., Warren, H. P., & Wang, Y.-M. 2004, ApJ, 616, 1224

Sheeley, N. R., et al. 1997, ApJ, 484, 472

Simnett, G. M. 2004, A&A, 416, 759

Vourlidas, A., Howard, R. A., Morrill, J. S., & Munz, S. 2002, in COSPAR Colloq. Ser. 14, Solar-Terrestrial Magnetic Activity and Space Environment, ed. H. Wang & R. Xu (Boston: Pergamon), 201

Wang, Y.-M., & Sheeley, N. R. 2006, ApJ, 650, 1172 (Paper I)

Wang, Y.-M., Sheeley, N. R., Howard, R. A., Rich, N. B., & Lamy, P. L. 1999, Geophys. Res. Lett., 26, 1349

Wang, Y.-M., et al. 1998, ApJ, 498, L165